RSC Advances

PAPER

View Article Online
View Journal | View Issue

Cite this: *RSC Adv.*, 2018, **8**, 12641

A series of Ln_4^{III} clusters: Dy_4 single molecule magnet and Tb_4 multi-responsive luminescent sensor for Fe^{3+}, $CrO_4^{2-}/Cr_2O_7^{2-}$ and 4-nitroaniline†

Yaru Qin, Yu Ge, Shasha Zhang, Hao Sun, Yu Jing, Yahong Li * and Wei Liu

Received 17th February 2018
Accepted 26th March 2018

DOI: 10.1039/c8ra01485j

rsc.li/rsc-advances

Five tetranuclear lanthanide clusters of compositions $[Ln_4L_4(NO_3)_2(Piv)_2]\cdot 2CH_3OH$ (Ln = Gd (**1**), Tb (**2**), Dy (**3**), Ho (**4**), Er (**5**); H_2L = 2-(((2-hydroxy-3-methoxybenzyl)imino)methyl)-6-methoxyphenol; Piv = pivalic acid) were synthesized under solvothermal conditions. The structures of **1–5** were characterized by single-crystal X-ray crystallography. Complexes **1–5** possess a zig-zag topology with $[Ln_4O_6]$ cores being formed by the fusion of oxygen atom-bridged two $[Ln_2O_2]$ moieties. Direct-current magnetic susceptibility studied in the 2–300 K range revealed weak antiferromagnetic interactions in **1**, **2**, **4**, **5** and ferromagnetic interactions in **3**. Complex **3** exhibits single molecule magnet (SMM) behavior. The luminescence studies indicated that complex **2** can serve as highly sensitive and selective luminescent materials for Fe^{3+}, CrO_4^{2-}, $Cr_2O_7^{2-}$ and 4-nitroaniline (4-NA), demonstrating that complex **2** should be a potential candidate for multi-responsive luminescent sensor.

Introduction

Polynuclear lanthanide clusters have been attracting considerable attention due to their fascinating structures[1] as well as potential applications in single molecule magnets (SMMs),[2] luminescent devices[3] and magnetocaloric materials.[4] SMMs are of considerable promise as molecular spintronic devices for high-density data storage.[5] The significant anisotropy of lanthanides arising from large unquenched orbital angular momentum[2a,2u] has made lanthanides to be attractive candidates for SMMs. Recently, the research efforts towards lanthanide SMMs have been devoted to polynuclear complexes with variable nuclearities.[2] Moreover, owing to the characteristic sharp emission peaks, a large Stokes shift and a wide emission range, the utilization of lanthanide complexes as luminescent materials, particularly luminescent sensor,[6] also attracts intensive interest.

Fe^{3+} ion plays an important role in industry and in various metabolic processes.[7] However, excessive Fe^{3+} ion probably leads to some diseases, such as Alzheimer's disease, due to production of reactive oxygen species (ROS).[8] CrO_4^{2-} and $Cr_2O_7^{2-}$ ions can cause severe environment pollution,[9] gemmulation, renal failure, lung cancer, and skin allergy by prolonged exposure.[10] Nitroaromatic compounds (NACs), *e.g.*, nitroaromatic (NB), 4-nitrophenol (4-NP), 4-nitroaniline (4-NA), 4-nitrotoluene (4-NT), 4-nitrochlorobenzene (4-Cl-NB), 2,4-dinitrotoluene (2,4-DNT), 2,4-dinitrophenol (2,4-DNP), *etc.*, are threatening human life.[11] Thus, it is of high importance to develop fast and facile methods for detecting those ions and compounds. A number of fluorescence-based sensing materials based on metal–organic frameworks (MOFs),[12] coordination polymers,[13] and mononuclear compounds[14] have been utilized to detect specific target inorganic anions, cations or organic molecules, due to high efficiency, selectivity and simplicity. Whereas, luminescent sensors base on lanthanide polynuclear clusters were rarely studied. The recent advances in this area indicated that they are potential sensors for nitroaromatic explosive compounds[15] and F^- ion.[16]

We are interested in designing and synthesizing Ln^{III} clusters supported by *o*-vanillin-containing Schiff base ligand 2-(((2-hydroxy-3-methoxybenzyl)imino)methyl)-6-methoxyphenol (H_2L) and pivalic acid. The selection of both H_2L and pivalic acid as the ligands is based on the following considerations. (i) The combination of the *o*-vanillin-based ligand and pivalic acid fosters the formation of polynuclear clusters owing to the incorporation of the phenolic oxygen atoms from the H_2L ligand with the carboxylate group from pivalic acid. (ii) H_2L is an electron rich π-conjugated multidentate organic ligand, which can act as antennae to sensitize the weak luminescent metal centres, such as Tb(III). (iii) Although the single molecule magnet behaviours of a series of Ln^{III} clusters have been studied, their multiple fluorescence detection abilities towards

College of Chemistry, Chemical Engineering and Materials Science, Soochow University, Suzhou 215123, China. E-mail: liyahong@suda.edu.cn

† Electronic supplementary information (ESI) available: CCDC 1538938 (**1**), 1538931 (**2**), 1538932 (**3**), 1538933 (**4**) and 1538934 (**5**). For ESI and crystallographic data in CIF or other electronic format see DOI: 10.1039/c8ra01485j

Fe^{3+}, $CrO_4^{2-}/Cr_2O_7^{2-}$, and NACs have not been reported. In this work, five tetranuclear lanthanide clusters of compositions $[Ln_4L_4(NO_3)_2(Piv)_2]\cdot 2CH_3OH$ (Ln = Gd (**1**), Tb (**2**), Dy (**3**), Ho (**4**), Er (**5**)) supported by H_2L were synthesized *via* solvothermal method. Complexes **1–5** possess $[Ln_4O_6]$ cores formed by the fusion of two phenoxide oxygen-bridged two $[Ln_2O_2]$ moieties. The magnetic studies indicated antiferromagnetic interactions in **1**, **2**, **4** and **5**. Complex **3** exhibits typical single molecule magnet behaviour. The luminescent sensing properties of **2** for selective and sensitive detections of Fe^{3+}, $CrO_4^{2-}/Cr_2O_7^{2-}$ ions in aqueous solutions and 4-NA in ethanol solutions were also investigated. The low detection limits and high quenching constants K_{SV} indicate that complex **2** may potentially be considered as a multi-responsive luminescence-based sensor for quantitative and highly sensitive detections of 4-NA, Fe^{3+} and $CrO_4^{2-}/Cr_2O_7^{2-}$ ions.

Experimental section

Synthesis of 2-(((2-hydroxy-3-methoxybenzyl)imino)methyl)-6-methoxyphenol (H_2L)

All solvents and regents were of analytical grade and used as received without further purification. 3-Methoxysalicylamine was prepared according to the reported procedure.[17] A solution of methoxysalicylaldehyde (20 mmol) in ethanol was added to a solution of 3-methoxysalicylamine (20 mmol) in 15 mL ethanol. After the reaction mixture was stirred at room temperature for 4 hours, yellow precipitates were formed. The yellow precipitates were isolated, washed with hexane and dried in vacuum to afford the product as a yellow solid (Scheme 1). Yield: 4.76 g (83%). ^{1}H NMR (600 MHz, chloroform-d) δ 8.38 (s, 1H), 6.90–6.84 (m, 3H), 6.83–6.74 (m, 3H), 4.82 (s, 2H), 3.87 (s, 3H), 3.85 (s, 3H). ^{13}C NMR (151 MHz, chloroform-d) δ 165.57, 152.66, 148.63, 146.39, 143.48, 123.64, 123.01, 121.34, 119.66, 118.56, 117.50, 113.90, 109.89, 56.60, 56.06, 56.04. Elemental anal. calcd for $C_{16}H_{17}NO_4$: C, 66.89; H, 5.96; N, 4.88%. Found: C, 66.77; H, 6.23; N, 5.18%. Selected IR data (KBr, cm^{-1}): 3400(w), 1630(m), 1593(w), 1487(m), 1474(s), 1461(m), 1440(m), 1351(w), 1315(w), 1277(m), 1249(s), 1237(s), 1216(m), 1188(m), 1162(m), 1074(m), 993(m), 979(m), 903(m), 842(w), 830(w), 801(w), 785(w), 738(s), 760(s), 743(s), 734(s), 710(w).

Physical measurement

Elemental analyses for C, H, and N were carried out with a Perkin-Elmer 2400 analyser. Fourier transform (FT) IR spectra were recorded with a Bruker VERTEX 70 FTIR spectrophotometer in the range of 600–4000 cm^{-1}. Magnetic susceptibility measurements were performed in the temperature range of 2–300 K, using a Quantum Design MPMS XL-7 SQUID magnetometer. Powder X-ray diffraction (PXRD) was obtained from a Rigaku D/Max-2500 diffractometer at 40 kV and 100 mA with a Cu-target tube and a graphite monochromator. Fluorescence spectra for the samples were recorded on a FLS-920 fluorescence spectrophotometer. The UV-Vis absorption spectra were determined with an Agilent Cary-60 spectra photometer at room temperature. X-ray photoelectron spectroscopy (XPS) experiments were carried out by a ESCALAB 250Xi spectrometer using an Al Kα source at room temperature.

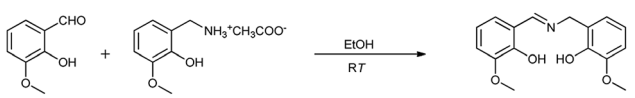

Scheme 1 Synthesis of the H_2L ligand.

X-ray single-crystal data collection and structure determination

The diffraction data for **1–5** were collected on a Bruker D8-VENTURE (120 K) CCD X-ray diffractometer equipped with a graphite monochromated Mo Kα radiation (λ = 0.71073 Å). The ω–2θ scan technique was applied. The crystal structures of all complexes were solved with the Olex2 solve solution program[18] using Intrinsic Phasing and refined by full-matrix least-squares minimization using the ShelXL refinement package.[19] All H atoms were placed on appropriate positions in theory and their positions were refined using the riding model. The details of the crystal parameters, data collection and refinements for the complexes are summarized in Table 1. Selected bond lengths and angles with their estimated standard deviations are listed in Table S1.†

Synthesis of 1–5

A mixture of $Ln(NO_3)_3\cdot 6H_2O$ (Ln = Gd, Tb, Dy, Ho, Er) (0.1 mmol), H_2L (0.1 mmol), pivalic acid (0.1 mmol), triethylamine (0.2 mmol) and CH_3OH (2.5 mL) was sealed in a pyrex-tube (10 mL). The tube was heated for 24 h at 80 °C. After cooling to room temperature, yellow block crystals suitably for X-ray diffraction analysis were obtained.

$[Gd_4L_4(NO_3)_2(Piv)_2]\cdot 2CH_3OH$ (1). Yield of **1** is 47% (0.0254 g) based on Gd. Elemental anal. calcd for $C_{76}H_{86}N_6O_{28}Gd_4$: C, 42.25; H, 4.01; N, 3.89%. Found: C, 42.44; H, 3.99; N, 4.12%. Selected IR data (KBr, cm^{-1}): 2955(m), 1621(m), 1548(m), 1468(s), 1420(m), 1403(m), 1323(w), 1296(w), 1271(m), 1245(s), 1228(m), 1166(m), 1062(m), 1028(m), 1013(m), 977(w), 951(w), 914(w), 867(m), 785(m), 735(s), 612(w).

$[Tb_4L_4(NO_3)_2(Piv)_2]\cdot 2CH_3OH$ (2). Yield of **2** is 53% (0.0287 g) based on Tb. Elemental anal. calcd for $C_{76}H_{86}N_6O_{28}Tb_4$: C, 42.12; H, 4.00; N, 3.88%. Found: C, 41.74; H, 4.04; N, 4.07%. Selected IR data (KBr, cm^{-1}): 2956(m), 1622(m), 1549(m), 1469(s), 1420(m), 1402(m), 1323(w), 1288(w), 1271(m), 1245(s), 1229(m), 1166(m), 1063(m), 1028(m), 1013(m), 978(w), 952(w), 914(w), 868(m), 785(m), 735(s), 612(w).

$[Dy_4L_4(NO_3)_2(Piv)_2]\cdot 2CH_3OH$ (3). Yield of **3** is 54% (0.0294 g) based on Dy. Elemental anal. calcd for $C_{76}H_{86}N_6O_{28}Dy_4$: C, 41.84; H, 3.97; N, 3.85%. Found: C, 41.84; H, 4.05; N, 3.95%. Selected IR data (KBr, cm^{-1}): 2956(m), 1623(m), 1550(m), 1470(s), 1420(m), 1403(m), 1324(w), 1289(w), 1271(m), 1245(s), 1230(m), 1166(m), 1063(m), 1029(m), 1014(m), 979(w), 953(w), 916(w), 868(m), 785(m), 735(s), 613(w).

$[Ho_4L_4(NO_3)_2(Piv)_2]\cdot 2CH_3OH$ (4). Yield of **4** is 53% (0.0290 g) based on Ho. Elemental anal. calcd for $C_{76}H_{86}N_6O_{28}Ho_4$: C, 41.66; H, 3.96; N, 3.84%. Found: C, 41.47; H, 4.05; N, 4.00%.

Table 1 Crystal data and structure refinements for **1–5**

	1	**2**	**3**	**4**	**5**
Empirical formula	$C_{76}H_{86}N_6O_{28}Gd_4$	$C_{76}H_{86}N_6O_{28}Tb_4$	$C_{76}H_{86}N_6O_{28}Dy_4$	$C_{76}H_{86}N_6O_{28}Ho_4$	$C_{76}H_{86}N_6O_{28}Er_4$
Formula weight	2160.50	2167.18	2181.50	2191.02	2200.54
Temperature/K	120	120	120	120	120
Crystal system	Monoclinic	Monoclinic	Monoclinic	Monoclinic	Monoclinic
Space group	$P2_1/c$	$P2_1/c$	$P2_1/c$	$P2_1/c$	$P2_1/c$
a/Å	13.4900(07)	13.4681(15)	13.457(03)	13.4321(16)	13.4131(7)
b/Å	11.9674(06)	11.9193(13)	11.905(02)	11.8480(14)	11.8637(7)
c/Å	24.5060(13)	24.483(3)	24.500(06)	24.450(3)	24.4580(14)
α/°	90	90	90	90	90
β/°	95.961(2)	95.984(4)	96.03	96.123(4)	96.222(2)
γ/°	90	90	90	90	90
Volume/Å^3	3934.9(9)	3908.9(7)	3903.1(07)	3868.9(8)	3869.1(4)
Z	2	2	2	2	2
ρ_{calc} g cm^{-3}	1.823	1.841	1.856	1.881	1.889
μ/mm^{-1}	3.413	3.661	3.872	4.133	4.381
F(000)	2128.0	2136.0	2144.0	2152.0	2160.0
Crystal size/mm^3	02 × 0.04 × 0.04	0.4 × 0.05 × 0.05	0.40 × 0.05 × 0.05	0.40 × 0.05 × 0.05	0.25 × 0.24 × 0.23
θ Range	2.28 to 27.502	2.287 to 27.565	2.928 to 27.488	2.501 to 27.63	2.394 to 27.605
Index ranges	$-17 \le h \le 17$, $-15 \le k \le 15$, $-31 \le l \le 29$	$-17 \le h \le 17$, $-15 \le k \le 15$, $-31 \le l \le 31$	$-17 \le h \le 17$, $-15 \le k \le 15$, $-26 \le l \le 31$	$-17 \le h \le 17$, $-15 \le k \le 15$, $-31 \le l \le 31$	$-17 \le h \le 16$, $-15 \le k \le 15$, $-28 \le l \le 31$
Reflections collected	59 585	60 747	53 678	59 835	60 923
Independent reflections	9047 [R (int) = 0.0954]	8987 [R (int) = 0.0456]	8994 [R (int) = 0.0408]	8938 [R (int) = 0.0803]	8920 [R (int) = 0.0483]
Data/restraints/parameters	9047/18/533	8987/12/533	8944/12/533	8938/12/533	8920/12/533
Goodness-of-fit on F^2	1.093	1.116	1.182	1.058	1.206
Final R indexes [$I \ge 2\sigma$ (I)]	$R_1 = 0.0428$, w$R_2 = 0.0616$	$R_1 = 0.0267$, w$R_2 = 0.0513$	$R_1 = 0.0311$, w$R_2 = 0.0531$	$R_1 = 0.0313$, w$R_2 = 0.0603$	$R_1 = 0.0329$, w$R_2 = 0.0546$
Final R indexes [all data]	$R_1 = 0.0737$, w$R_2 = 0.0682$	$R_1 = 0.0405$, w$R_2 = 0.0575$	$R_1 = 0.0383$, w$R_2 = 0.0549$	$R_1 = 0.0500$, w$R_2 = 0.0685$	$R_1 = 0.0413$, w$R_2 = 0.0563$
Largest diff. peak/hole/e Å^{-3}	0.81/−0.88	0.90/−0.77	0.85/−1.08	0.85/−1.10	0.93/−1.41

Selected IR data (KBr, cm^{-1}): 2956(m), 1623(m), 1551(m), 1471(s), 1421(m), 1403(m), 1325(w), 1290(w), 1272(m), 1245(s), 1231(m), 1166(m), 1063(m), 1030(m), 1014(m), 979(w), 953(w), 916(w), 868(m), 785(m), 736(s), 613(w).

$[Er_4L_4(NO_3)_2(Piv)_2]\cdot 2CH_3OH$ (5). Yield of **5** is 51% (0.0280 g) based on Er. Elemental anal. calcd for $C_{76}H_{86}N_6O_{28}Er_4$: C, 41.48; H, 3.94; N,3.82%. Found: C, 40.83; H, 4.03; N 3.93%. Selected IR data (KBr, cm^{-1}): 2956(m), 1623(m), 1552(m), 1471(s), 1421(m), 1402(m), 1326(w), 1290(w), 1272(m), 1243(s), 1231(m), 1166(m), 1063(m), 1030(m), 1014(m), 980(w), 953(w), 916(w), 868(m), 785(m), 736(s), 613(w).

Results and discussion

Synthesis of complexes

The tetranuclear complexes **1–5** were synthesized under solvothermal conditions. When a mixture of $Ln(NO_3)_3\cdot 6H_2O$ (Ln = Gd, Tb, Dy, Ho, Er), H_2L (the synthesis of H_2L was shown in Scheme 1), and pivalic acid, in a 1 : 1 : 1 molar ratio in MeOH/Et_3N was sealed in a Pyrex-tube and heated under solvothermal conditions, yellow block crystals were generated after being heated at 353 K for one day. The experimental powder X-ray diffraction patterns matched well with those simulated from the crystal structures, demonstrating the purity of complexes **1–5**.

Description of crystal structure of 1–5

Single crystal X-ray analyses and powder X-ray diffraction analyses indicated that complexes **1–5** are isostructural. They crystalize in the monoclinic $P2_1/c$ space group (Table 1, Fig. 1). Thus, complex **3** was chosen as a representative for **1–5** to describe the structure in detail. The molecular structure of **3** contains four Dy(III) ions in a zig-zag topology, four L^{2-} ligands, two deprotonated pivalic acids, two NO_3^- anions and two CH_3OH solvate molecules (Fig. 1). Two L^{2-} ligands coordinate in a μ_2: η^1, η^2, η^1, η^1 fashion whereas the other two L^{2-} ligands coordinate in a μ_3: η^1, η^2, η^1, η^2, η^1 mode (Scheme 2). The structure of **3** is composed by two asymmetric [Dy2] units which are connected by phenolate bridges from the Schiff base ligands with Dy⋯Dy distances of 3.697(2) Å (Dy1⋯Dy2) and 3.839(2) Å (Dy2⋯Dy2A). Dy1 centre is coordinated by two oxygen atoms (O1 and O3) from one ligand, one nitrogen atom (N1) from the same ligand, two oxygen atoms (O5 and O6) from another ligand set, two oxygen atoms (O11 and O12) from one NO_3^- ion, and one oxygen atom (O10) from a deprotonated pivalic acid, forming a NO7 coordination environment. Dy2 centre was coordinated by two oxygen atoms (O7 and O9) from one ligand, one nitrogen atom (N2) from the same ligand, four oxygen atoms (O7A, O8A, O1 and O2) from another two ligand sets and one oxygen atom (O9) from deprotonated pivalic acid. It also forms a NO7 coordination environment. The Dy1–O bond

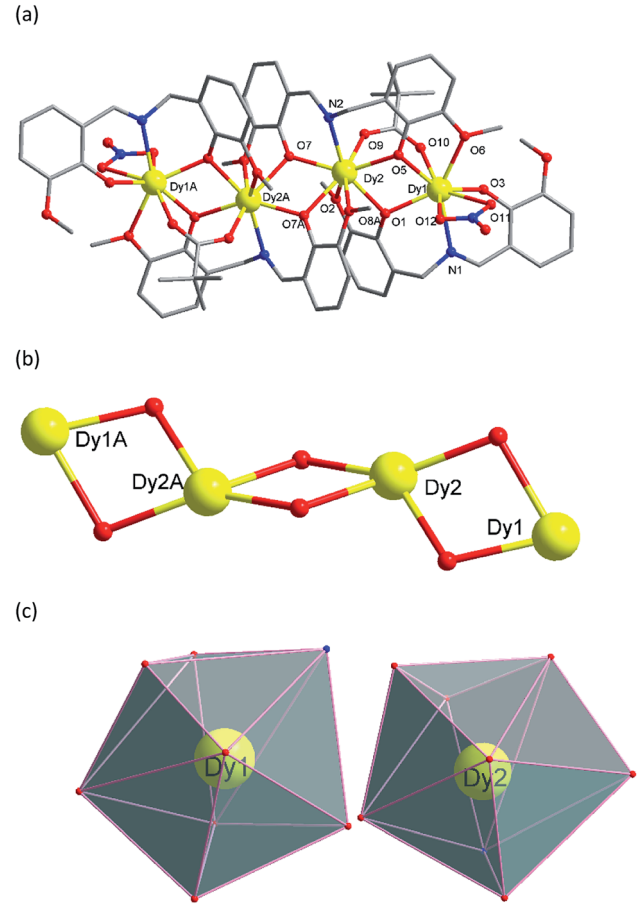

Fig. 1 (a) Molecular structure of **3**. Symmetry code: $A = 2 - X, -Y, 1 - Z$ (hydrogen atoms and solvents have been omitted for clarity). (b) The tetranuclear $[Dy_4O_6]$ core in **3**. (c) Coordination polyhedrons of Dy(III) ions in **3**.

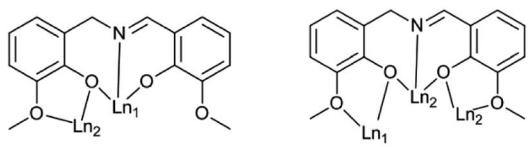

Scheme 2 The coordination modes of ligand (L^{2-}) in complexes **1–5**.

lengths are in the range of 2.169(3)–2.534(3) Å and the Dy1–N bond is 2.491(3) Å. The Dy2–O bond lengths are in the range of 2.249(3)–2.635(3) Å and the Dy2–N bond is 2.443(3) Å. They are all comparable to those of reported complexes with [DyNO7] units.[2o,20] The exact coordination geometries of the octa-coordinated Ln(III) ions were analysed by SHAPE 2.1 software[21] and resulting data were shown in Table S2.† The resulting data from the closer analysis reveal that Ln1(III) ion is in a square antiprism (D_{4d}) configuration while Ln2(III) is in a biaugmented trigonal prism (C_{2v}) configuration with a minimum continuous shape measures (CShM) value.

Magnetic studies

The magnetic properties of **1–5** were investigated by direct-current (DC) magnetic susceptibility studies under a magnetic field of 1000 Oe in the temperature range 2–300 K. The experimental $\chi_M T$ values at 300 K and magnetic behaviours of **1–5** are shown in Table 2. The $\chi_M T$ *versus* T plots for **1–5** are shown in Fig. 2. For **1**, the room temperature $\chi_M T$ value of 33.41 cm^3 K mol^{-1} is slightly higher than value of 31.52 cm^3 K mol^{-1} expected for four magnetically isolated Gd^{III} ions ($^8S_{7/2}$, $g = 2$). At 300 K, the $\chi_M T$ values of 46.91 and 58.50 cm^3 K mol^{-1} for complexes **2** and **3** are close to the expected values of 47.20 cm^3 K mol^{-1} for uncoupled Tb^{III} ions ($^7F_6$, $g = 2$) and 56.68 cm^3 K mol^{-1} for uncoupled Dy^{III} ions ($^8H_{15/2}$, $g = 4/3$). The room temperature $\chi_M T$ values for **4** and **5** are 57.47 and 44.21 cm^3 K mol^{-1}, respectively, which are slightly lower than values of 58.28 cm^3 K mol^{-1} expected for four magnetically uncoupled Ho^{III} ions ($^5I_8$, $g = 5/4$) and 45.92 cm^3 K mol^{-1} expected for four magnetically uncoupled Er^{III} ions ($^4I_{15/2}$, $g = 6/5$). Upon cooling, the $\chi_M T$ product of **1** stays almost constant in the temperature range of 300–30 K and then decreases rapidly, reaching minimum value of 13.80 cm^3 K mol^{-1} at 2 K. This magnetic behaviour suggests weak antiferromagnetic exchange interactions. The application of a Curie–Weiss law gives values of $\theta = -1.98$ K, $C = 32.86$ for **1** (Fig. S6†). With the decrease of temperature, the $\chi_M T$ values for **2**, **4** and **5** firstly decrease slowly and then decline sharply to minimum values at 2 K. The decrease of $\chi_M T$ values for **2**, **4** and **5** is typical for Ln^{III} ions and is due to several factors, namely, the thermal depopulation of the excited m_J sublevels of the $^{2s+1}\Gamma_J$ ground state of the Ln^{III} ion originated by a crystal field symmetry, in combination with the weak Ln^{III}–Ln^{III} antiferromagnetic interactions in **2**, **4** and **5**.[22]

Upon cooling, the $\chi_M T$ value of **3** decreases imperceptibly and reaches minimum value of 55.9 cm^3 K mol^{-1} at 23 K, which is attributed by the thermal depopulation of Stark effect for a single Dy^{III} ion. Continuous being cooled down to 2 K, the $\chi_M T$ product sharply increases to a maximum value of 69.6 cm^3 K mol^{-1}. This magnetic phenomenon may be caused by the presence of ferromagnetic interactions between the spin carriers.[2g,23]

To investigate the dynamic magnetic properties of **3**, alternating-current (ac) magnetic susceptibilities were determined under zero-dc field with a 2 Oe oscillating ac field (Fig. 3). The out-of-phase susceptibility (χ'') displays frequency-dependent phenomenon at low temperatures, which suggests the presence of slow relaxation of the magnetization, typical of SMM behaviour.[24] However, the peak maxima are not found. Ac susceptibility measurements of **3** under 0–10 000 Oe dc field at 1000 Hz were conducted (Fig. S7†). Unfortunately, no optimum field was found. The energy barrier (Ea/K_B) and pre-exponential factor (τ_0) values were calculated from the frequency-dependent ac susceptibility data by using the Debye model based on the equation $\ln(\chi''/\chi') = \ln(\omega\tau_0) + Ea/K_BT$.[24a] The best fitting results give $Ea/K_B \approx 1.61$ K and $\tau_0 \approx 7.42 \times 10^{-6}$ s (Fig. 4). Apparently, the τ_0 value is comparable to the expected values 10^{-6} to 10^{-11} for typical SMMs.[25]

Table 2 Direct-current (dc) magnetic susceptibilities of **1–5**

Complex	Metal ions	Theoretical $\chi_M T$/cm^3 K mol^{-1}	Experimental $\chi_M T$/cm^3 K mol^{-1} at 300 K	Magnetic behaviour
1	Gd	31.52	33.41	AF
2	Tb	47.20	46.91	AF
3	Dy	58.68	58.50	F
4	Ho	58.28	57.47	AF
5	Er	45.92	44.21	AF

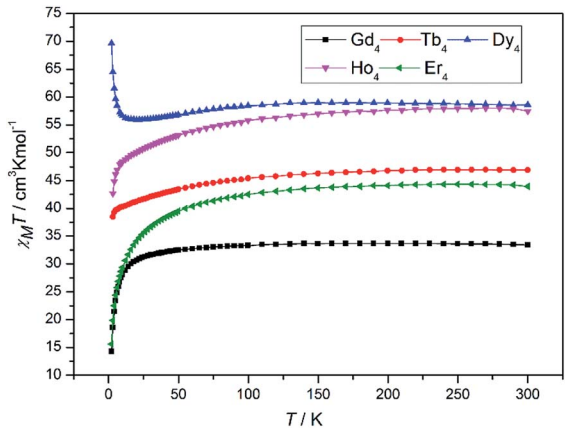

Fig. 2 Temperature dependence of the $\chi_M T$ products in the range of 2–300 K under 1000 Oe for **1–5**.

Luminescent properties

The solid-state luminescent properties of the H_2L ligand and **2** were measured at room temperature (Fig. S8†). The H_2L ligand displays a broad emission around 544 nm ($\lambda_{ex} = 467$ nm), which is due to the $\pi \rightarrow \pi^*$ transition between the ligand orbitals. Complex **1** exhibits a ligand-centred broad band emission at 557 nm and a shoulder at 483 nm ($\lambda_{ex} = 396$ nm), which is attributed to the ligand centred π–π^* and charge–transfer transition between ligands and metal centers[26] (Fig. S8b†). As shown in Fig. S8,† the solid-state emission spectra of **3–5** (Dy_4, Ho_4, Er_4) display emission bands centred at 482, 482, 480 nm respectively under excitation at 324 nm. The blue shifts of **3–5** are tentatively assigned to the electrostatic interaction between the ligand and metal ions.[26b] Complex **2** displays four characteristic emission peaks at 490, 544, 584, and 618 nm ($\lambda_{ex} = 360$ nm), corresponding to $^5D_4 \rightarrow {}^7F_6$, $^5D_4 \rightarrow {}^7F_5$, $^5D_4 \rightarrow {}^7F_4$ and $^5D_4 \rightarrow {}^7F_3$,[3b] respectively (Fig. S9†). The strongest emission of **2** at 544 nm is responsible for the green emission, which can be observed with the naked eyes. The π-conjugated multidentate organic ligand can act as antennae to sensitize the weak luminescent of Tb(III). Therefore, the strong and sharp luminescence emission of **2** can be visually observed, which allows it to be considered as a fluorescent sensor. The results of the luminescence sensing experiments revealed that complex **2** can be served as a luminescent senior for selectively sensing 4-NA, Fe^{3+}, CrO_4^{2-} and $Cr_2O_7^{2-}$.

In order to examine the stability, the PXRD patterns of **2** were measured after being soaked in aqueous solutions with different pH values for several days. The PXRD patterns remained almost unaltered and agreed well with the simulated pattern, revealing the excellent stability of **2** in different solutions (Fig. S10 and S11†). Twenty samples of **2** (2 mg/2 ml suspension) after detection of 4-NA (2 mL, 1×10^{-3}), Fe^{3+} (1 mL, 3×10^{-3}), CrO_4^{2-} (2 mL, 2×10^{-3}) and $Cr_2O_7^{2-}$ (2 mL, 2×10^{-3}) were filtered and dried to recover for PXRD test.

Detection of metal ions

Based on the fact that compound **2** possesses excellent stability in the aqueous solutions with broad pH range, its potential florescent sensing properties towards metal ions were investigated. Firstly, a series of aqueous solutions of **2** were prepared by adding 2 mg of complex **2** into 2 mL of deionized water. Then, the resulting suspensions were sonicated for 8, 10 and 30 minutes, respectively. The sizes of suspensions of particles of **2** were analysed by scanning electron microscopy. The size-distribution histograms were obtained from measuring the

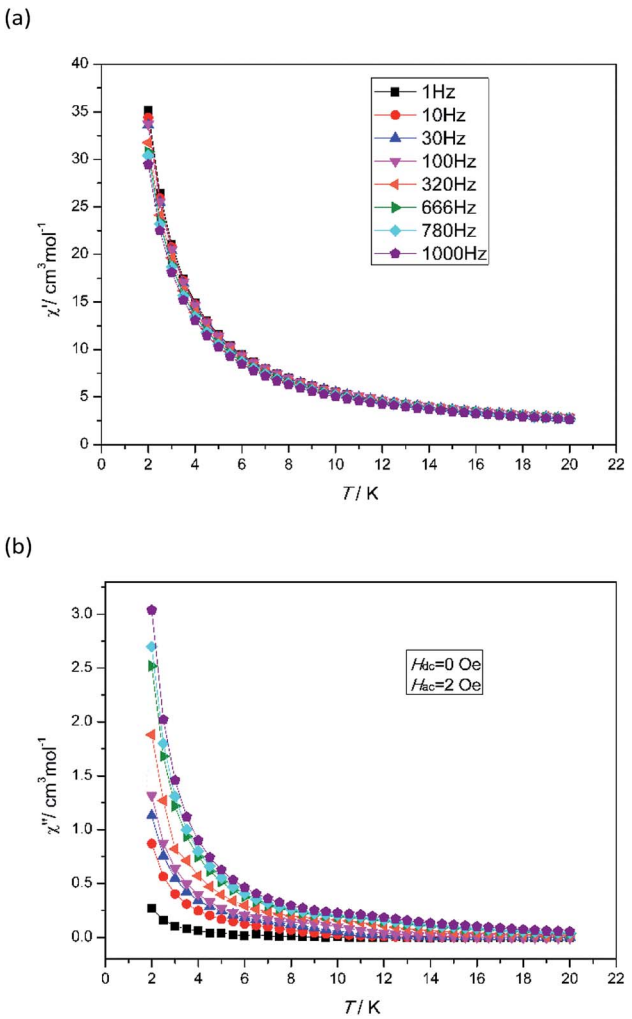

Fig. 3 Temperature dependence of the in-phase χ' (a) and out-of-phase χ'' (b) for **3** under zero dc field at different frequencies in the range of 2–20 K.

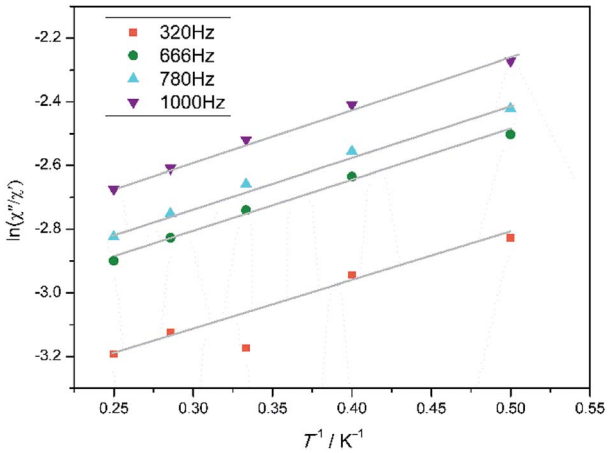

Fig. 4 Plots of ln (χ''/χ') *vs.* T^{-1} for **3** in the range 2–4.0 K. The grey solid lines correspond to the best fit result.

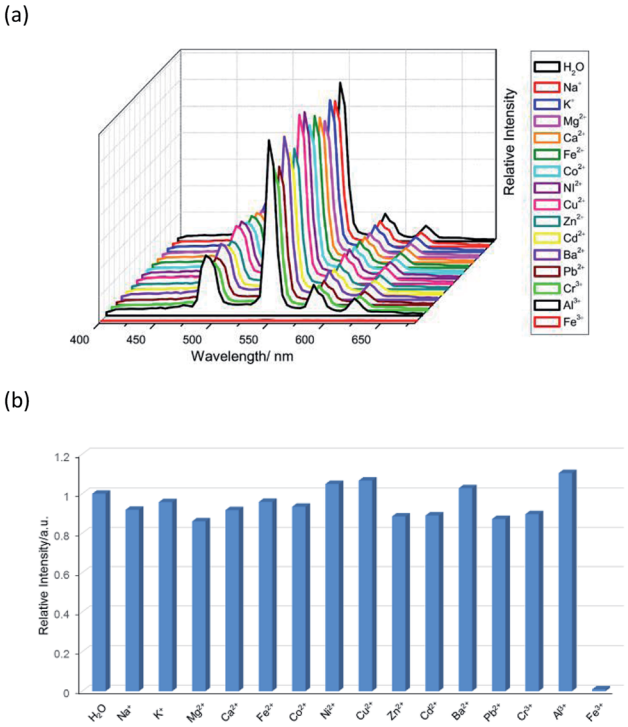

Fig. 5 (a) The emission spectra and (b) relative intensities at 544 nm ($^5D_4 \rightarrow {}^7F_5$) for **2** which was dispersed in aqueous solutions of different metal ions upon excitation at 360 nm.

diameters of 100 randomly selected particles. According to the histograms of the particle size distributions in Fig. S12,† the average diameters of **2** after being sonicated for 8, 15 and 30 minutes are estimated to be approximately 15.58 ± 3.02, 12.75 ± 2.30 and 7.77 ± 2.62 μm, respectively, of which the sample (**2**) after being sonicated for 30 minutes displays the smallest particle size. The smaller size of the **2** leading to larger surface areas and more accessible active sites on their surface would be beneficial to realize highly sensitive and fast-response luminescent sensing.[27]

Therefore, the resulting suspensions were sonicated for 30 minutes. Next, aqueous solutions of nitrate salts (200 μL, 10^{-2} M) of Na^+, K^+, Mg^{2+}, Ca^{2+}, Fe^{2+}, Co^{2+}, Ni^{2+}, Cu^{2+}, Zn^{2+}, Cd^{2+}, Pb^{2+}, Al^{3+}, Cr^{3+} and Fe^{3+} were added in the above suspensions for fluorescence testing. As shown in Fig. 5, the metal salts slightly altered the luminescent intensity of **2**, whereas Fe^{3+} ion exhibited a significant influence on the luminescence of **2**. Concentration-based studies were performed by adding different amount of aqueous solutions of Fe^{3+} ion into the suspensions of complex **2** (2 mg in 2 mL deionized water). As shown in Fig. 6, the luminescent intensities of **2** progressively decreased as the concentrations of Fe^{3+} ion increased. The luminescent intensities and the concentrations of Fe^{3+} ions show good linear relationships at low concentrations. The limit of detection (LOD) value is calculated to be 1×10^{-5} M by $3\delta/s$, where δ is the standard deviation of fluorescent test for 10 blank measurements and s is the slope of the calibration curve (Fig. S13b†).[12i,j] In addition, the quenching effect can be explained by the Stern–Volmer equation: $I_0/I = K_{SV}[Q] + 1$, where I_0 and I are the luminescent intensities before and after addition of the target analyte, respectively. K_{SV} is the Stern–Volmer quenching constant (M^{-1}) and $[Q]$ is the concentration of the analyte.[12p] As can be seen from Fig. S13a,† the Stern–Volmer (SV) plot for Fe^{3+} ion displays nearly linear relationships at low concentration with K_{SV} value of 1.86×10^4 M^{-1}, which is comparable to those of reported fluorescent sensors based on Ln-complexes (Table S3†). The S–V plot deviates from linearity at high concentration (Fig. 6b), which may be attributed to both the occurrence of static and dynamic quenching. Nonlinear S–V curve of **2** can be fitted well by an exponential quenching equation, $I_0/I = 2.118 \exp(4.327[Fe^{3+}]) + 0.199$. The possible interference experiments were carried out for complex **2**. The selectivity of **2** towards Fe^{3+} ion over other metal cations was verified by adding Fe^{3+} ion (10^{-2} M, 0.2 mL) to the suspensions of **2** (2.4 mL) in which other competitive metal ions (10^{-2} M, 0.2 mL) were introduced. Then the changes of the emission intensities were recorded. No obvious changes were observed, which suggested that fluorescence detection of **2** could not be interfered by the presence of other cations. Competitive experiments indicated that **2** has great potential as a highly selective sensor for Fe^{3+} ion (Fig. 7). To study the recycling performance of the fluorescent sensor, Fe^{3+} ion (10^{-2} M, 0.2 mL) was introduced to the suspension of complex **2** (2 mL), then washed by water (after Fe^{3+} ion being detected) with five cycles of sensing experiments. As shown in Fig. 8, the fluorescent intensity of the samples did not drop significantly after five cycles. The resulting K_{SV}, LOD value, high selectivity, stability and recyclable property reveal that complex **2** can be considered as a fluorescent sensor for Fe^{3+} ion in aqueous system.

As reported, the possible fluorescence quenching mechanism for **2** towards Fe^{3+} ion mainly rises from three aspects: (a) the collapse of the structure;[28] (b) the weak interactions between Fe^{3+} ion and the methoxy group at the terminal of **2**;[29] (c) the energy transfer between **2** and Fe^{3+} ion.[30] In order to understand which part was the main contributor, the PXRD, X-ray photoelectron spectroscopy (XPS) and UV-Vis absorption spectra of

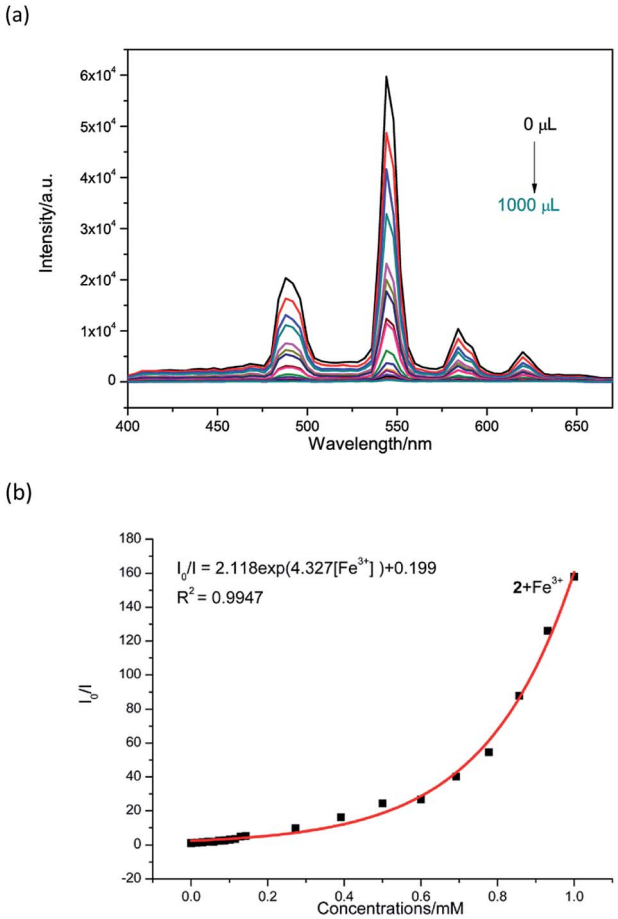

Fig. 6 (a) Luminescent responses of a water suspension of **2** (2 mg mL^{-1}) towards different concentrations of Fe^{3+} ions (3×10^{-3} M, 0–1000 μL). (b) Nonlinear Stern–Volmer (SV) plot for Fe^{3+} in the presence of a water suspension of **2** (2 mg/2 mL).

analytes were determined. By comparing the PXRD pattern (Fig. S15†) of **2** before and after the detection of Fe^{3+} ion, we found that no obvious changes occurred in this process, which indicated that the structure of **2** did not shatter. Depending on the result of the PXRD patterns, the fluorescence quenching mechanism of structural collapse can be ruled out. As shown in XPS spectrum of **2** (Fig. S14†), after the detection of Fe^{3+} ion, the

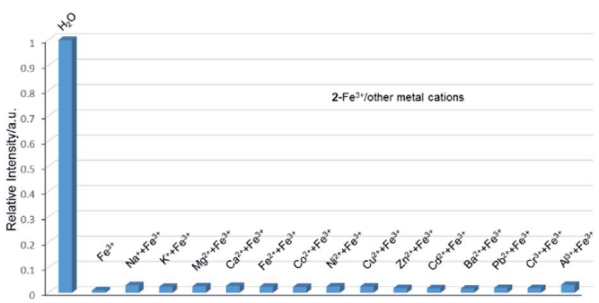

Fig. 7 Relative luminescent intensities of the suspensions of **2** at 544 nm treated with Fe^{3+} in the presence of the other metal ions in water.

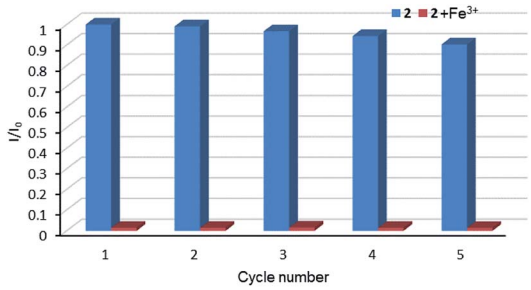

Fig. 8 Relative luminescent intensity for $^5D_4 \rightarrow {}^7F_5$ transition of suspension of **2** in the absence and presence of Fe^{3+} for each cyclic test.

O1s peak did not change, demonstrating the nonexistence of the weak interactions between Fe^{3+} ion and complex **2**. However, as shown in Fig. S14,† the absorption band of Fe^{3+} ion from 250 nm to 400 nm remarkably overlaps the excitation band of **2** from 300 to 400 nm. Consequently, the solution of Fe^{3+} may absorb the energy of the excitation wavelength, which leads to the luminescence quenching.

Detection of anions

The aqueous solutions (200 μL, 10^{-2} M) of common sodium salts Na_yX (X = F^-, Cl^-, Br^-, I^-, NO_3^-, OAc^-, SCN^-, SO_4^{2-}, CO_3^{2-}, $Cr_2O_7^{2-}$, CrO_4^{2-}, and PO_4^{3-} were added in the suspensions of **2** (2 mg complex **2** in 2 mL water, and then being sonicated for 30 minutes) to investigate the luminescence quenching effects. An alluring finding is that CrO_4^{2-} and $Cr_2O_7^{2-}$ ions showed remarkable turnoff quenching effect on florescent intensities of **2**, whereas other tested anions displayed minor effects on the luminescent intensity (Fig. 9). In order to further investigate the sensitivity of **2** toward CrO_4^{2-} and $Cr_2O_7^{2-}$, we implemented the titration experiments by adding aqueous solutions of CrO_4^{2-} or $Cr_2O_7^{2-}$ (2×10^{-3} M) to the suspension of complex **2** (2 mg in 2 mL water). The emission titration data were collected. As expected, the fluorescent intensity of **2** gradually decreased with the increase of the concentrations of CrO_4^{2-} or $Cr_2O_7^{2-}$ (Fig. S16†). Moreover, the S–V curve of **2** (Fig. 10) can be fitted well by an exponential quenching equation, $I_0/I = 0.897 \exp(2.801[CrO_4^{2-}]) + 0.135$ for CrO_4^{2-} and $I_0/I = 2.601 \exp(2.807[Cr_2O_7^{2-}]) - 1.747$ for $Cr_2O_7^{2-}$. The S–V plot shows good linear relationships at low concentrations (Fig. S17a and S17b†), suggesting that both static and dynamic quenching may happen simultaneously. The quenching constants, K_{SV}, are calculated to be 2.998×10^3 M^{-1} (CrO_4^{2-}) and 7.44×10^3 M^{-1} ($Cr_2O_7^{2-}$) for **2** (Fig. S17a and S17b†). The LOD values calculated according to $3\delta/s$ reach 5.2×10^{-5} M (CrO_4^{2-}) and 2.7×10^{-5} M ($Cr_2O_7^{2-}$) for **2** (Fig. S17c and S17d†). Competitive experiments were carried out to study the interference of other ions on the fluorescent sensitivity for **2** towards CrO_4^{2-} or $Cr_2O_7^{2-}$ ions. The fluorescent intensity decreased significantly after adding CrO_4^{2-} or $Cr_2O_7^{2-}$ (0.2 mL, 10^{-2} M) into suspensions of **2** (2 mg in 2.2 mL water), in which other anions (0.2 mL, 10^{-2} M) were also added (Fig. 11). Moreover, recyclability experiments on the detection of CrO_4^{2-}

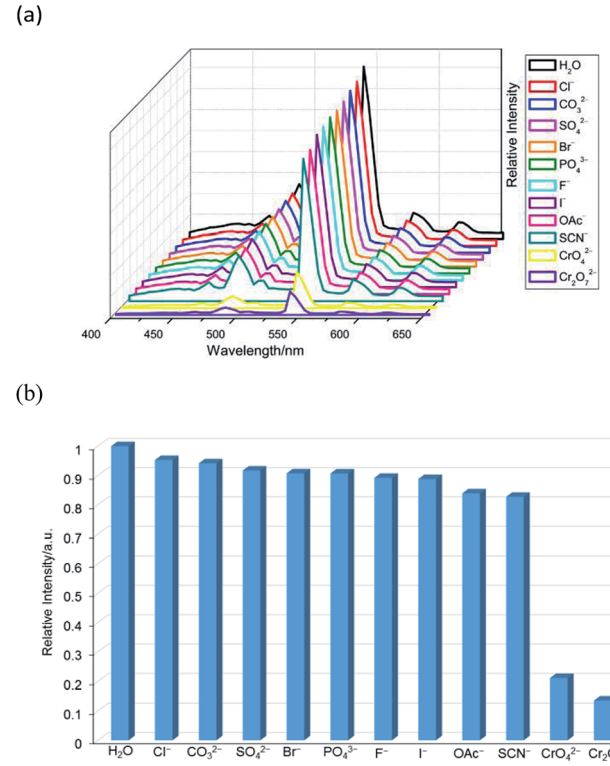

Fig. 9 (a) The emission spectra and (b) relative intensities at 544 nm ($^5D_4 \rightarrow {}^7F_5$) for **2** dispersed in different anion aqueous solutions upon excitation at 360 nm.

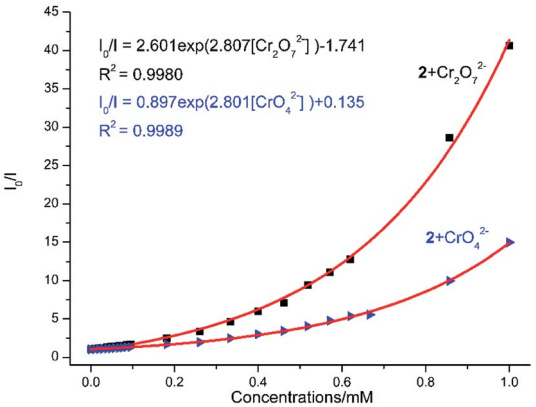

Fig. 10 Nonlinear Stern–Volmer (SV) plot for CrO_4^{2-}/$Cr_2O_7^{2-}$ in the presence of a water suspension of **2** (2 mg/2 mL).

or $Cr_2O_7^{2-}$ were performed. After five cycles of quenching experiments and regenerations, the quenching efficiency experiences only a minor decrease (Fig. 12). These results showed that complex **2** could be a potential candidate for sensitive and selective detections of CrO_4^{2-} or $Cr_2O_7^{2-}$ ions. A comparison of florescent sensing properties based on **2**, Ln-MOF, and Ln-CP towards Fe^{3+}, CrO_4^{2-} or $Cr_2O_7^{2-}$ ions is listed in Table S3.†[6b,12f–o,13a]

After CrO_4^{2-} and $Cr_2O_7^{2-}$ ions were detected, the PXRD patterns of **2** were measured. The obtained PXRD patterns still

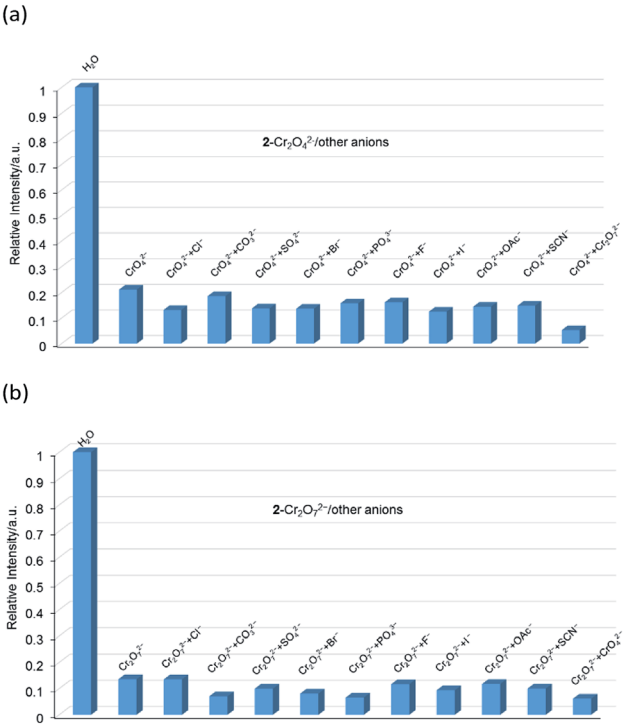

Fig. 11 (a) Relative luminescent intensities of the suspension of **2** at 544 nm treated with CrO_4^{2-} in the presence of the other anions in water. (b) Relative luminescent intensities of the suspension of **2** at 544 nm treated with $Cr_2O_7^{2-}$ in the presence of the other anions in water.

well correspond with the original data of **2**, which demonstrate that the crystal structure of **2** is retained (Fig. S20†). On the other hand, the UV-Vis spectra of CrO_4^{2-} and $Cr_2O_7^{2-}$ ions in aqueous solution were determined. As shown in Fig. 13, the absorption bands of CrO_4^{2-} in the range of 230–450 nm and $Cr_2O_7^{2-}$ in the range of 275–475 nm display extensive overlap with the excitation band of **2**. Therefore, luminescence quenching can be attributed to reducing the efficiency of the energy transfer from the ligand to the lanthanide ions, as the energy of the excitation light will be strongly absorbed by CrO_4^{2-} or $Cr_2O_7^{2-}$.[6b,13e]

Detection of nitrobenzene derivatives

Complex **2** was dispersed in ethanol and then stirred for three days. It was filtered and dried. The PXRD of **2** (Fig. S20†) after being stirred for three days matched with that of the simulated data, which indicated that complex **2** was stable in ethanol solution. The stable nature of **2** in ethanol solution affords a prerequisite for the detection of nitroaromatics (NACs). Nitrobenzene (NB), 4-nitrophenol (4-NP), 4-nitroaniline (4-NA), 4-nitrotoluene (4-NT), 4-nitrochlorobenzene (4-Cl-NB), 2,4-dinitrotoluene (2,4-DNT) and 2,4-dinitrophenol (2,4-DNP) were selected to explore the potential of **2** as a chemosensor in ethanol solution. Firstly, complex **2** (2 mg) was homogeneously dispersed in a series of ethanol solution (2 mL) and sonicated for 30 minutes to form a uniform suspension. Then, different

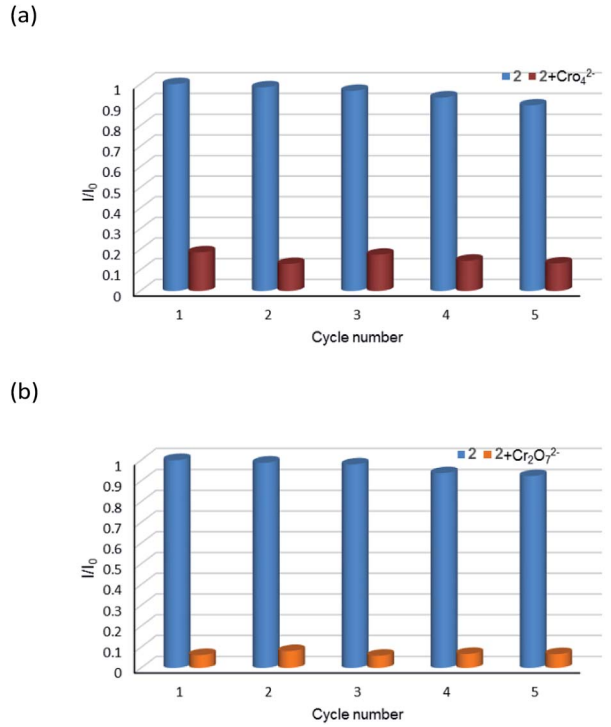

Fig. 12 Relative luminescence intensity for $^5D_4 \rightarrow {}^7F_5$ transition of a suspension of **2** in the absence and presence of CrO_4^{2-} anions (a) and $Cr_2O_7^{2-}$ anions (b) for each cyclic test.

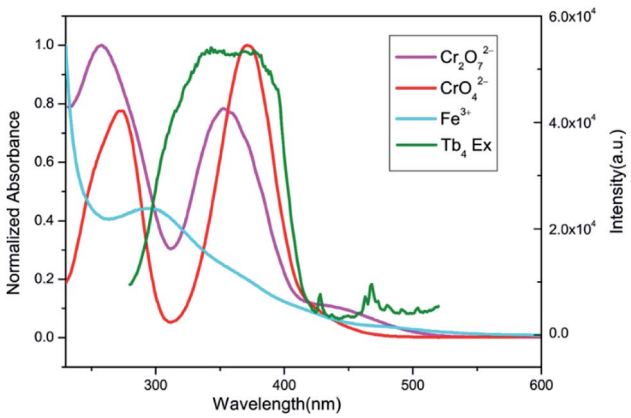

Fig. 13 Spectral overlap between normalized absorption spectra of solutions of Fe^{3+}, CrO_4^{2-}, $Cr_2O_7^{2-}$ ions and excitation spectrum of **2** in water.

NACs (10 μL, 10^{-1} M) was added to the above-mentioned suspensions, respectively. Next, the fluorescent intensities of the resulting mixture were measured. As shown in Fig. 14, the order of quenching extend is as follows: 4-NA > 2,4-DNP > 4-NP > 4-NT > NB > 4-Cl-NB > 2,4-DNT. Concentration-dependent titration experiments of 4-NA were performed to test the influence of concentrations on fluorescent intensity. As the concentration of 4-NA increases, the fluorescent intensity gradually decreased (Fig. S18†). The liner fitting of the S–V plot for 4-NA at low concentrations (Fig. S19a†) gives K_{SV} value of 1.14×10^4 M^{-1} (4-NA). Nonlinear concentration curve (Fig. 15)

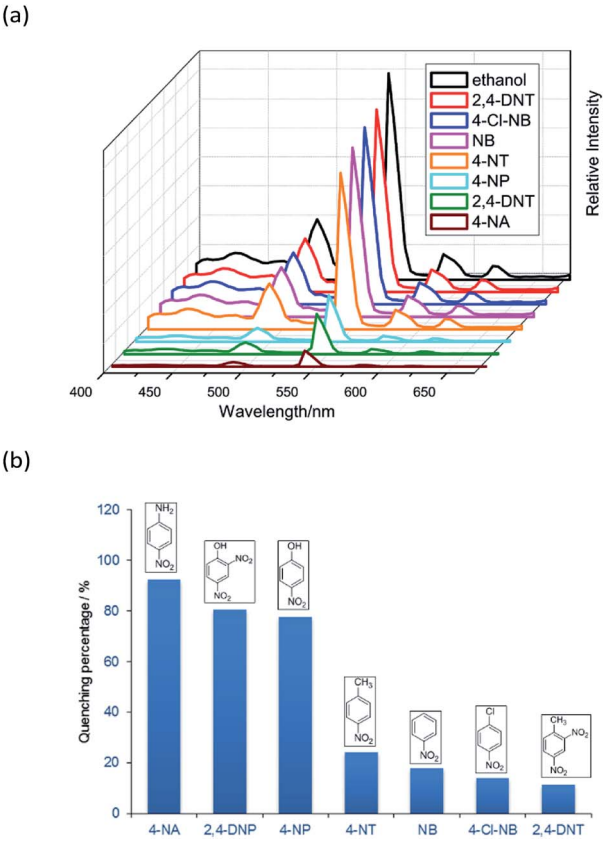

Fig. 14 (a) The emission spectra and (b) luminescence quenching at 544 nm ($^5D_4 \rightarrow {}^7F_5$) for the suspensions of **2** in the presence of seven different ethanol solutions of NACs (10 μL, 10^{-1} M) upon excitation at 360 nm.

can be fitted well by an exponential quenching equation: $I_0/I = 3.776 \exp(5.380[Q]) - 3.131$ (Q = 4-NA). The detection limit value (Fig. S19b†) towards 4-NA was calculated by $3\delta/s$, generating 1.17 ppm (8.5×10^{-6} M) for **2**. Recyclability experiments on the detection of 4-NA were performed. After five cycles of quenching experiments and regenerations, the quenching efficiency experiences only a minor decrease (Fig. 16). To our knowledge, few fluorescent complexes acted as sensors for 4-NA in ethanol system have been reported in the literature

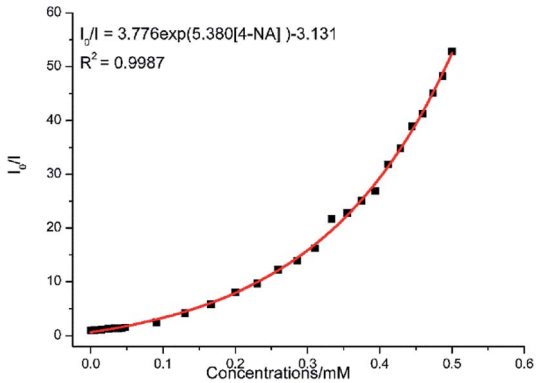

Fig. 15 Nonlinear Stern–Volmer (SV) plot for 4-NA in the presence of an ethanol suspension of **2** (2 mg/2 mL).

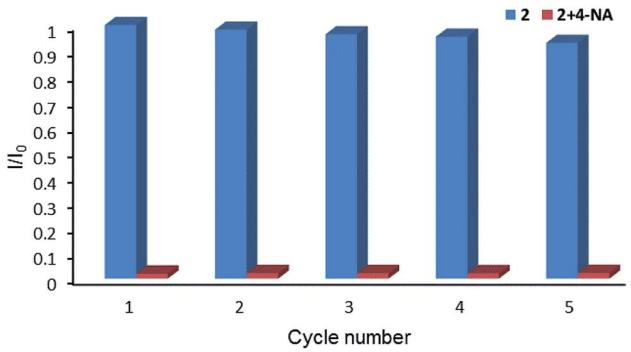

Fig. 16 Relative luminescence intensity for $^5D_4 \rightarrow {}^7F_5$ transition of ethanol suspension of **2** in the absence and presence of 4-NA for each cyclic test.

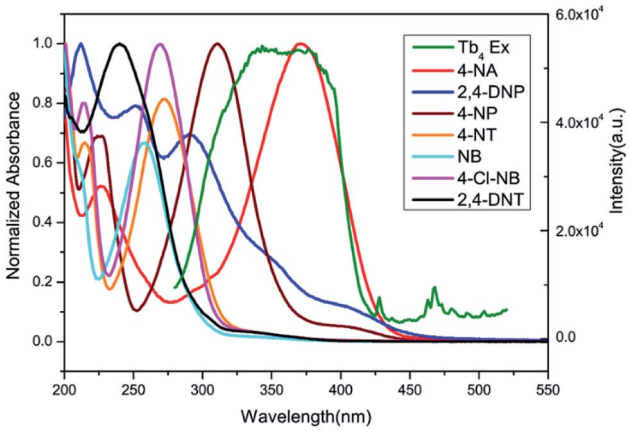

Fig. 17 Spectral overlap between normalized absorption spectra of seven selected NACs and excitation spectra of **2** in ethanol solution.

(Table S4†).[12q–s,13b] Compared to luminescent sensors based on transition metal complexes, lanthanide complex **2** has the advantage of characteristic emissions and bright luminescent colour of Tb(III) ion. No lanthanide clusters as sensors for 4-NA have been reported.

As reported, the quenching mechanism of NACs sensors is ascribed to two factors: photo-induced electron transfer (PET) and resonance energy transfer (RET) or their cooperative effect. According to the molecular orbital theory, nitroaromatic compounds are good electron acceptors, due to the substitution of the electron-withdrawing nitro groups on the aromatic ring, which can stabilize the lowest unoccupied molecular orbital (LUMO) of the system *via* conjugation effect, ultimately leading to the complete or part quenching of luminescence-based sensor.[13b,31] The electron transfer originated from the phenyl rings of the ligands of **2** to excellent electron donor nitrobenzene leads to luminescence quenching upon excitation. On the other hand, the UV-Vis results reveal that there are obvious overlaps between the absorption spectrum of NACs especially 4-NA and the emission spectrum of **2** (Fig. 17). This would permit energy transfer from **2** to NACs, thus further improving the luminescence quenching efficiency towards NACs.[30b]

Conclusions

In summary, five tetranuclear lanthanide clusters have been synthesized by using $Ln(NO_3)_3 \cdot 6H_2O$ (Ln = Gd, Tb, Dy, Ho, Er), pivalic acid and Schiff base ligand 2-(((2-hydroxy-3-methoxybenzyl)imino)methyl)-6-methoxyphenol (H_2L) as starting materials under solvothermal method. Complexes **1–5** possess $[Ln_4O_6]$ cores formed by the fusion of two phenoxide oxygen bridged two $[Ln_2O_2]$ moieties. The magnetic properties of **1–5** were investigated. Antiferromagnetic interactions were determined for **1**, **2**, **4** and **5**. Complex **3** displayed typical single molecule magnet behaviour. Considering its low detection limits and high quenching constant K_{sv}, complex **2** may potentially be utilized as luminescence sensors for quantitative detection of 4-NA, Fe^{3+} and $CrO_4^{2-}/Cr_2O_7^{2-}$ ions. Although the design of chemosensors is more based on academic or research interest, the exceptional stability of Tb_4 clusters makes it applicable to extreme industrial application.

Conflicts of interest

There are no conflicts to declare.

Acknowledgements

The authors appreciate the financial support from Natural Science Foundation of China (21272167, 21772140), Natural Science Foundation of Jiangsu Province of China (BK20171213), a Project Funded by the Priority Academic Program Development of Jiangsu Higher Education Institution and the project of scientific and technologic infrastructure of Suzhou (SZS201708).

References

1 (*a*) X. Y. Zheng, Y. H. Jiang, G. L. Zhuang, D. P. Liu, H. G. Liao, X. J. Kong, L. S. Long and L. S. Zheng, *J. Am. Chem. Soc.*, 2017, **139**, 18178–18181; (*b*) X.-Y. Zheng, J.-B. Peng, X.-J. Kong, L.-S. Long and L.-S. Zheng, *Inorg. Chem. Front.*, 2016, **3**, 320–325; (*c*) Z. Zheng, *Chem. Commun.*, 2001, 2521–2529.

2 (*a*) Y. N. Guo, G. F. Xu, W. Wernsdorfer, L. Ungur, Y. Guo, J. Tang, H. J. Zhang, L. F. Chibotaru and A. K. Powell, *J. Am. Chem. Soc.*, 2011, **133**, 11948–11951; (*b*) J. Long, F. Habib, P. H. Lin, I. Korobkov, G. Enright, L. Ungur, W. Wernsdorfer, L. F. Chibotaru and M. Murugesu, *J. Am. Chem. Soc.*, 2011, **133**, 5319–5328; (*c*) F. Habib, G. Brunet, V. Vieru, I. Korobkov, L. F. Chibotaru and M. Murugesu, *J. Am. Chem. Soc.*, 2013, **135**, 13242–13245; (*d*) P. H. Lin, T. J. Burchell, R. Clerac and M. Murugesu, *Angew. Chem., Int. Ed.*, 2008, **47**, 8848–8851; (*e*) F. Tuna, C. A. Smith, M. Bodensteiner, L. Ungur, L. F. Chibotaru, E. J. McInnes, R. E. Winpenny, D. Collison and R. A. Layfield, *Angew. Chem., Int. Ed.*, 2012, **51**, 6976–6980; (*f*) J. Zhang, H. Zhang, Y. Chen, X. Zhang, Y. Li, W. Liu and Y. Dong, *Dalton Trans.*, 2016, **45**, 16463–16470; (*g*) L. Zhang, J. Jung, P. Zhang, M. Guo, L. Zhao, J. Tang and B. Le Guennic,

Chem.–Eur. J., 2016, **22**, 1392–1398; (*h*) Y. Qin, H. Zhang, H. Sun, Y. Pan, Y. Ge, Y. Li and Y.-Q. Zhang, *Chem.–Asian J.*, 2017, **12**, 2834–2844; (*i*) M. Gysler, F. El Hallak, L. Ungur, R. Marx, M. Hakl, P. Neugebauer, Y. Rechkemmer, Y. Lan, I. Sheikin, M. Orlita, C. E. Anson, A. K. Powell, R. Sessoli, L. F. Chibotaru and J. van Slageren, *Chem. Sci.*, 2016, **7**, 4347–4354; (*j*) X. L. Li, H. Li, D. M. Chen, C. Wang, J. Wu, J. Tang, W. Shi and P. Cheng, *Dalton Trans.*, 2015, **44**, 20316–20320; (*k*) J. Tang, I. Hewitt, N. T. Madhu, G. Chastanet, W. Wernsdorfer, C. E. Anson, C. Benelli, R. Sessoli and A. K. Powell, *Angew. Chem., Int. Ed.*, 2006, **45**, 1729–1733; (*l*) P. H. Guo, J. L. Liu, Z. M. Zhang, L. Ungur, L. F. Chibotaru, J. D. Leng, F. S. Guo and M. L. Tong, *Inorg. Chem.*, 2012, **51**, 1233–1235; (*m*) H. L. Gao, X. P. Zhou, Y. X. Bi, H. Y. Shen, W. M. Wang, N. N. Wang, Y. X. Chang, R. X. Zhang and J. Z. Cui, *Dalton Trans.*, 2017, **46**, 4669–4677; (*n*) P. P. Yang, X. F. Gao, H. B. Song, S. Zhang, X. L. Mei, L. C. Li and D. Z. Liao, *Inorg. Chem.*, 2011, **50**, 720–722; (*o*) G. Abbas, Y. Lan, G. E. Kostakis, W. Wernsdorfer, C. E. Anson and A. K. Powell, *Inorg. Chem.*, 2010, **49**, 8067–8072; (*p*) A. K. Jami, V. Baskar and E. C. Sanudo, *Inorg. Chem.*, 2013, **52**, 2432–2438; (*q*) R. J. Blagg, C. A. Muryn, E. J. McInnes, F. Tuna and R. E. Winpenny, *Angew. Chem., Int. Ed.*, 2011, **50**, 6530–6533; (*r*) H. Zhang, R. Liu, J. Zhang, Y. Li, W. Liu and Y. Dong, *Chem.–Asian J.*, 2017, **12**, 507–514; (*s*) L. Qin, Y. Z. Yu, P. Q. Liao, W. Xue, Z. Zheng, X. M. Chen and Y. Z. Zheng, *Adv. Mater.*, 2016, **28**, 10772–10779; (*t*) S. T. Liddle and J. van Slageren, *Chem. Soc. Rev.*, 2015, **44**, 6655–6669; (*u*) P. Zhang, Y.-N. Guo and J. Tang, *Coord. Chem. Rev.*, 2013, **257**, 1728–1763.

3 (*a*) J. Mao, *Coord. Chem. Rev.*, 2007, **251**, 1493–1520; (*b*) E. C. Mazarakioti, K. M. Poole, L. Cunha-Silva, G. Christou and T. C. Stamatatos, *Dalton Trans.*, 2014, **43**, 11456–11460; (*c*) P. Bag, C. K. Rastogi, S. Biswas, S. Sivakumar, V. Mereacre and V. Chandrasekhar, *Dalton Trans.*, 2015, **44**, 4328–4340; (*d*) K. Su, F. Jiang, M. Wu, J. Qian, J. Pang, D. Yuan and M. Hong, *CrystEngComm*, 2016, **18**, 4921–4928.

4 (*a*) J.-L. Liu, Y.-C. Chen, F.-S. Guo and M.-L. Tong, *Coord. Chem. Rev.*, 2014, **281**, 26–49; (*b*) F. S. Guo, J. D. Leng, J. L. Liu, Z. S. Meng and M. L. Tong, *Inorg. Chem.*, 2012, **51**, 405–413; (*c*) A. Adhikary, J. A. Sheikh, S. Biswas and S. Konar, *Dalton Trans.*, 2014, **43**, 9334–9343; (*d*) J. B. Peng, X. J. Kong, Q. C. Zhang, M. Orendac, J. Prokleska, Y. P. Ren, L. S. Long, Z. Zheng and L. S. Zheng, *J. Am. Chem. Soc.*, 2014, **136**, 17938–17941; (*e*) K. Wang, Z. L. Chen, H. H. Zou, K. Hu, H. Y. Li, Z. Zhang, W. Y. Sun and F. P. Liang, *Chem. Commun.*, 2016, **52**, 8297–8300.

5 (*a*) R. Sessoli, D. Gatteschi, A. Caneschi and M. A. Nonvak, *Nature*, 1993, **365**, 141–143; (*b*) L. Bogani and W. Wernsdorfer, *Nat. mater.*, 2008, **7**, 179–186.

6 (*a*) B. V. Harbuzaru, A. Corma, F. Rey, J. L. Jorda, D. Ananias, L. D. Carlos and J. Rocha, *Angew. Chem., Int. Ed.*, 2009, **48**, 6476–6479; (*b*) J. Liu, G. Ji, J. Xiao and Z. Liu, *Inorg. Chem.*, 2017, **56**, 4197–4205; (*c*) J. Sahoo, R. Arunachalam, P. S. Subramanian, E. Suresh, A. Valkonen, K. Rissanen and M. Albrecht, *Angew. Chem., Int. Ed.*, 2016, **55**, 9625–9629.

7 (*a*) X. liu and E. C. Theil, *Acc. Chem. Res.*, 2005, **38**, 167–175; (*b*) K. P. Carter, A. M. Young and A. E. Palmer, *Chem. Rev.*, 2014, **114**, 4564–4601; (*c*) A. Barba-Bon, A. M. Costero, S. Gil, M. Parra, J. Soto, R. Martinez-Manez and F. Sancenon, *Chem. Commun.*, 2012, **48**, 3000–3002.

8 (*a*) M. A. Lovellac, J. D. Robertsons, W. J. Teesclaleb, J. L. Campbellb and W. R. Markesberycd, *J. Neurol. Sci.*, 1998, **158**, 47–52; (*b*) D. L. Jiang, X. J. Li, R. Williams, S. Patel, L. J. Men, Y. S. Wang and F. M. Zhou, *Biochemistry*, 2009, **48**, 7939–7947.

9 (*a*) V. K. Gupta, M. Gupta and S. Sharma, *Water Res.*, 2001, **35**, 1125–1134; (*b*) C. Ozdemir, S. Dursun, M. E. Argun and S. Dogan, *Environ. Technol.*, 2005, **26**, 397–400; (*c*) G. Hilson, *Sci. Total Environ.*, 2006, **362**, 1–14; (*d*) M. Bansal, D. Singh and V. K. Garg, *J. Hazard. Mater.*, 2009, **171**, 83–92.

10 (*a*) C. Cervantes, J. Campos-García, S. Devars, F. Gutiérrez-Corona, H. Loza-Tavera, J. C. Torres-Guzmán and R. Moreno-Sánchez, *FEMS Microbiol. Rev.*, 2001, **25**, 335–347; (*b*) A. Zhitkovich, Y. Song, G. Quievryn and V. Voitkun, *Biochemistry*, 2001, **40**, 549–560; (*c*) K. R. Manygoats, M. Yazzie and D. M. Stearns, *J. Biol. Inorg Chem.*, 2002, **7**, 791–798; (*d*) A. Shanker, C. Cervantes, H. Loza-Tavera and S. Avudainayagam, *Environ. Int.*, 2005, **31**, 739–753; (*e*) K. L. Witt, M. D. Stout, R. A. Herbert, G. S. Travlos, G. E. Kissling, B. J. Collins and M. J. Hooth, *Toxicol. Pathol.*, 2013, **41**, 326–342; (*f*) C. M. Thompson, C. R. Kirman, D. M. Proctor, L. C. Haws, M. Suh, S. M. Hays, J. G. Hixon and M. A. Harris, *J. Appl. Toxicol.*, 2014, **34**, 525–536.

11 (*a*) Y. Salinas, R. Martinez-Manez, M. D. Marcos, F. Sancenon, A. M. Costero, M. Parra and S. Gil, *Chem. Soc. Rev.*, 2012, **41**, 1261–1296; (*b*) X. Sun, Y. Wang and Y. Lei, *Chem. Soc. Rev.*, 2015, **44**, 8019–8061; (*c*) G. R. Lotufo, J. D. Farrar, L. S. Inouyr, T. S. Bridges and D. B. Ringelberg, *Environ. Toxicol. Chem.*, 2001, **20**, 1762–1771.

12 (*a*) W. P. Lustig, S. Mukherjee, N. D. Rudd, A. V. Desai, J. Li and S. K. Ghosh, *Chem. Soc. Rev.*, 2017, **46**, 3242–3285; (*b*) Y. Cui, B. Chen and G. Qian, *Coord. Chem. Rev.*, 2014, **273–274**, 76–86; (*c*) L. E. Kreno, K. Leong, O. K. Farha, M. Allendorf, R. P. Van Duyne and J. T. Hupp, *Chem. Rev.*, 2012, **112**, 1105–1125; (*d*) B. Gole, A. K. Bar and P. S. Mukherjee, *Chem.–Eur. J.*, 2014, **20**, 13321–13336; (*e*) G.-Y. Wang, C. Song, D.-M. Kong, W.-J. Ruan, Z. Chang and Y. Li, *J. Mater. Chem. A*, 2014, **2**, 2213–2220; (*f*) K.-M. Wang, L. Du, Y.-L. Ma, J.-S. Zhao, Q. Wang, T. Yan and Q.-H. Zhao, *CrystEngComm*, 2016, **18**, 2690–2700; (*g*) W. Yan, C. Zhang, S. Chen, L. Han and H. Zheng, *ACS Appl. Mater. Interfaces*, 2017, **9**, 1629–1634; (*h*) R. Li, X.-L. Qu, Y.-H. Zhang, H.-L. Han and X. Li, *CrystEngComm*, 2016, **18**, 5890–5900; (*i*) X. H. Zhou, L. Li, H. H. Li, A. Li, T. Yang and W. Huang, *Dalton Trans.*, 2013, **42**, 12403–12409; (*j*) X. L. Zhao, D. Tian, Q. Gao, H. W. Sun, J. Xu and X. H. Bu, *Dalton Trans.*, 2016, **45**, 1040–1046; (*k*) M. Chen, W.-M. Xu, J.-Y. Tian, H. Cui, J.-X. Zhang, C.-S. Liu and M. Du, *J. Mater. Chem. C*, 2017, **5**, 2015–2021; (*l*) Z. Sun,

M. Yang, Y. Ma and L. Li, *Cryst. Growth Des.*, 2017, **17**, 4326–4335; (*m*) G. X. Wen, M. L. Han, X. Q. Wu, Y. P. Wu, W. W. Dong, J. Zhao, D. S. Li and L. F. Ma, *Dalton Trans.*, 2016, **45**, 15492–15499; (*n*) G. P. Li, G. Liu, Y. Z. Li, L. Hou, Y. Y. Wang and Z. Zhu, *Inorg. Chem.*, 2016, **55**, 3952–3959; (*o*) X. H. Huang, L. Shi, S. M. Ying, G. Y. Yan, L. H. Liu, Y. Q. Sun and Y. P. Chen, *CrystEngComm*, 2018, **20**, 189–197; (*p*) W. Liu, X. Huang, C. Xu, C. Chen, L. Yang, W. Dou, W. Chen, H. Yang and W. Liu, *Chem.–Eur. J.*, 2016, **22**, 18769–18776; (*q*) X.-Y. Wan, F.-L. Jiang, C.-P. Liu, K. Zhou, L. Chen, Y.-L. Gai, Y. Yang and M.-C. Hong, *J. Mater. Chem. A*, 2015, **3**, 22369–22376; (*r*) F. Wang, C. Wang, Z. Yu, Q. He, X. Li, C. Shang and Y. Zhao, *RSC Adv.*, 2015, **5**, 70086–70093; (*s*) F. Wang, Z. Yu, C. Wang, K. Xu, J. Yu, J. Zhang, Y. Fu, X. Li and Y. Zhao, *Sens. Actuators, B*, 2017, **239**, 688–695.

13 (*a*) W. Gao, F. Liu, B. Y. Zhang, X. M. Zhang, J. P. Liu, E. Q. Gao and Q. Y. Gao, *Dalton Trans.*, 2017, **46**, 13878–13887; (*b*) L. Huo, J. Zhang, L. Gao, X. Wang, L. Fan, K. Fang and T. Hu, *CrystEngComm*, 2017, **19**, 5285–5292; (*c*) X. Zhang, X. Luo, N. Zhang, J. Wu and Y.-Q. Huang, *Inorg. Chem. Front.*, 2017, **4**, 1888–1894; (*d*) W. J. Gong, R. Yao, H. X. Li, Z. G. Ren, J. G. Zhang and J. P. Lang, *Dalton Trans.*, 2017, **46**, 16861–16871; (*e*) Y. Lin, X. Zhang, W. Chen, W. Shi and P. Cheng, *Inorg. Chem.*, 2017, **56**, 11768–11778.

14 (*a*) N. Shao, J. Jin, G. Wang, Y. Zhang, R. Yang and J. Yuan, *Chem. Commun.*, 2008, 1127–1129; (*b*) L.-L. Wen, X.-G. Hou, G.-G. Shan, W.-L. Song, S.-R. Zhang, H.-Z. Sun and Z.-M. Su, *J. Mater. Chem. C*, 2017, **5**, 10847–10854; (*c*) B. Y. Man, D. S. Chan, H. Yang, S. W. Ang, F. Yang, S. C. Yan, C. M. Ho, P. Wu, C. M. Che, C. H. Leung and D. L. Ma, *Chem. Commun.*, 2010, **46**, 8534–8536; (*d*) J. P. Leonard and T. Gunnlaugsson, *J. Fluoresc.*, 2005, **15**, 585–595; (*e*) Y. Zhang, Z. Liu, Y. Zhang, Y. Xu, H. Li, C. Wang, A. Lu and S. Sun, *Sens. Actuators, B*, 2015, **211**, 449–455.

15 X. Z. Li, L. P. Zhou, L. L. Yan, D. Q. Yuan, C. S. Lin and Q. F. Sun, *J. Am. Chem. Soc.*, 2017, **139**, 8237–8244.

16 W. Chen, X. Tang, W. Dou, B. Wang, L. Guo, Z. Ju and W. Liu, *Chem.–Eur. J.*, 2017, **23**, 9804–9811.

17 I. Zagol-Ikapitte, V. Amernath, M. Bala, L. J. Roberts II, J. A. Oates and O. Boutaud, *Chem. Res. Toxicol.*, 2010, **23**, 240–250.

18 (*a*) O. V. Dolomanov, L. J. Bourhis, R. J. Gildea, J. A. K. Howard and H. Puschmann, *J. Appl. Crystallogr.*, 2009, **42**, 339–341; (*b*) G. M. Sheldrick, *Acta Cryst. A*, 2008, **64**, 112–122.

19 G. M. Sheldrick, *Acta Cryst. A*, 2015, **71**, 3–8.

20 (*a*) K. Zhang, D. Liu, V. Vieru, L. Hou, B. Cui, F. S. Guo, L. F. Chibotaru and Y. Y. Wang, *Dalton Trans.*, 2017, **46**, 638–642; (*b*) H. M. Dong, H. Y. Li, Y. Q. Zhang, E. C. Yang and X. J. Zhao, *Inorg. Chem.*, 2017, **56**, 5611–5622; (*c*) Y.-X. Zhang, M. Li, B.-Y. Liu, Z.-L. Wu, H.-Y. Wei and W.-M. Wang, *RSC Adv.*, 2017, **7**, 55523–55535.

21 D. Casanova, M. Llunell, P. Alemany and S. Alvarez, *Chem.–Eur. J.*, 2005, **11**, 1479–1494.

22 S. Das, A. Dey, S. Biswas, E. Colacio and V. Chandrasekhar, *Inorg. Chem.*, 2014, **53**, 3417–3426.

23 S. Mukherjee, J. Lu, G. Velmurugan, S. Singh, G. Rajaraman, J. Tang and S. K. Ghosh, *Inorg. Chem.*, 2016, **55**, 11283–11298.

24 (*a*) B. Peng, X. J. Kong, Y. P. Ren, L. S. Long, R. B. Huang and L. S. Zheng, *Inorg. Chem.*, 2012, **51**, 2186–2190; (*b*) L. Zhao, S. Xue and J. Tang, *Inorg. Chem.*, 2012, **51**, 5994–5996.

25 D. N. Woodruff, R. E. Winpenny and R. A. Layfield, *Chem. Rev.*, 2013, **113**, 5110–5148.

26 (*a*) L. Shen, L. Yang, Y. Fan, L. Wang and J. Xu, *CrystEngComm*, 2015, **17**, 9363–9369; (*b*) M. D. Allendorf, C. A. Bauer, R. K. Bhaktaa and R. J. T. Houk, *Chem. Soc. Rev.*, 2009, **38**, 1330–1352; (*c*) M. Kurmoo, *Chem. Soc. Rev.*, 2009, **38**, 1353–1379; (*d*) Y. J. Cui, Y. F. Yue, G. D. Qian and B. L. Chen, *Chem. Rev.*, 2012, **112**, 1126–1162.

27 (*a*) H. Xu, J. Gao, X. Qian, J. Wang, H. He, Y. Cui, Y. Yang, Z. Wang and G. Qian, *J. Mater. Chem. A*, 2016, **4**, 10900–10905; (*b*) M. Zhao, Y. Wang, Q. Ma, Y. Huang, X. Zhang, J. Ping, Z. Zhang, Q. Lu, Y. Yu and H. Xu, *Adv. Mater.*, 2015, **27**, 7372–7378; (*c*) H. He, S. H. Chen, D. Y. Zhang, R. Hao, C. Zhang, E. C. Yang and X. J. Zhao, *Dalton Trans.*, 2017, **46**, 13502–13509.

28 S. Dang, E. Ma, Z.-M. Sun and H. Zhang, *J. Mater. Chem.*, 2012, **22**, 16920–16926.

29 F. L. Hu, Y. X. Shi, H. H. Chen and J. P. Lang, *Dalton Trans.*, 2015, **44**, 18795–18803.

30 (*a*) S. Zhang, J. Yang, H. Wu, Y.-Y. Liu and J.-F. Ma, *Chem.–Eur. J.*, 2015, **21**, 15806–15819; (*b*) Y.-J. Yang, M.-J. Wang and K.-L. Zhang, *J. Mater. Chem. C*, 2016, **4**, 11404–11418.

31 J. H. Qin, H. R. Wang, M. L. Han, X. H. Chang and L. F. Ma, *Dalton Trans.*, 2017, **46**, 15434–15442.